nature medicine

A Gpr120-selective agonist improves insulin resistance and chronic inflammation in obese mice

Da Young Oh[1], Evelyn Walenta[1], Taro E Akiyama[2], William S Lagakos[1], Denise Lackey[1], Ariane R Pessentheiner[1,3], Roman Sasik[1], Nasun Hah[4], Tyler J Chi[1], Jason M Cox[2], Mary Ann Powels[2], Jerry Di Salvo[2], Christopher Sinz[2], Steven M Watkins[5], Aaron M Armando[6], Heekyung Chung[1], Ronald M Evans[4,7], Oswald Quehenberger[1,6], Joanne McNelis[1], Juliane G Bogner-Strauss[3] & Jerrold M Olefsky[1]

It is well known that the ω–3 fatty acids (ω–3-FAs; also known as *n*–3 fatty acids) can exert potent anti-inflammatory effects[1–4]. Commonly consumed as fish products, dietary supplements and pharmaceuticals, ω–3-FAs have a number of health benefits ascribed to them, including reduced plasma triglyceride levels, amelioration of atherosclerosis and increased insulin sensitivity[5–7]. We reported that Gpr120 is the functional receptor for these fatty acids and that ω–3-FAs produce robust anti-inflammatory, insulin-sensitizing effects, both *in vivo* and *in vitro*, in a Gpr120-dependent manner[8]. Indeed, genetic variants that predispose to obesity and diabetes have been described in the gene encoding GPR120 in humans (*FFAR4*)[9]. However, the amount of fish oils that would have to be consumed to sustain chronic agonism of Gpr120 is too high to be practical, and, thus, a high-affinity small-molecule Gpr120 agonist would be of potential clinical benefit. Accordingly, Gpr120 is a widely studied drug discovery target within the pharmaceutical industry. Gpr40 is another lipid-sensing G protein–coupled receptor[10], and it has been difficult to identify compounds with a high degree of selectivity for Gpr120 over Gpr40 (ref. 11). Here we report that a selective high-affinity, orally available, small-molecule Gpr120 agonist (cpdA) exerts potent anti-inflammatory effects on macrophages *in vitro* and in obese mice *in vivo*. Gpr120 agonist treatment of high-fat diet–fed obese mice causes improved glucose tolerance, decreased hyperinsulinemia, increased insulin sensitivity and decreased hepatic steatosis. This suggests that Gpr120 agonists could become new insulin-sensitizing drugs for the treatment of type 2 diabetes and other human insulin-resistant states in the future.

Gpr120 and Gpr40 are both lipid-sensing G protein–coupled receptors (GPCRs)[10,12], but although there is limited homology between these two polyunsaturated fatty acid (PUFA) receptors, identification of ligands that are highly selective for Gpr120 over Gpr40 has been challenging[11,13–15]. We have generated a small-molecule Gpr120 agonist, compound A (cpdA) (**Fig. 1a**), and have examined its selectivity for Gpr120 compared to Gpr40 using a Ca^{2+} FLIPR (fluorometric imaging plate reader) assay (**Fig. 1b**). We found that cpdA was fully selective for Gpr120 (log of the half-maximum effective concentration (EC_{50}) = −7.62 ± 0.11 M) with negligible activity toward Gpr40 (**Fig. 1b**). Gpr120 couples to Gαq/Gα11-initiated signal transduction pathways, and we therefore assessed the activity of cpdA in an inositol-1,4,5-triphosphate (IP_3) production assay, employing HEK 293 cells that stably express human or mouse Gpr120. The Gpr120 agonist produced concentration-dependent increases in IP_3 production from both human and mouse Gpr120–expressing cells (**Fig. 1c**).

In addition to promoting signaling via Gαq/11, Gpr120 also directly couples to β-arrestin-2 (refs. 8,14). Therefore, we examined the potency of cpdA in a β-arrestin-2 recruitment assay (**Fig. 1d**). We found that cpdA led to a concentration-dependent response to recruit β-arrestin-2 in both human and mouse Gpr120–expressing cells, with EC_{50}s of ~0.35 μM (**Fig. 1d**). As Gpr120 is a Gαq/11-coupled receptor, it stimulates both protein kinase C and mitogen-activated protein kinase, and both of these biological effects can be detected in a serum response element (SRE)-driven reporter system[8]. We transiently transfected HEK 293 cells with a plasmid construct encoding mouse Gpr120 and another plasmid encoding an SRE-luciferase promoter-reporter (SRE-luc). We treated the Gpr120:SRE-luc reporter cells with either docosahexaenoic acid (DHA) or cpdA. Gpr120 stimulation by cpdA was ~50-fold more sensitive than that achieved by DHA (**Fig. 1e**). We used DHA and cpdA at 100 μM and 10 μM, respectively, in all subsequent studies to achieve maximal effects.

In our previous studies[8], we showed that Gpr120 stimulation mediated anti-inflammatory responses in macrophages. To link these observations to cpdA, we evaluated the effect of DHA and cpdA on nuclear factor-κB (NF-κB) response element–driven reporter gene activity in wild-type (WT) and Gpr120-knockout primary mouse macrophages.

[1]Division of Endocrinology and Metabolism, Department of Medicine, University of California, San Diego, La Jolla, California, USA. [2]Merck Research Laboratories, Kenilworth, New Jersey, USA. [3]Institute of Biochemistry, Graz University of Technology, Graz, Austria. [4]Gene Expression Laboratory, Salk Institute for Biological Studies, La Jolla, California, USA. [5]Lipomics Technologies, West Sacramento, California, USA. [6]Department of Pharmacology, University of California, San Diego, La Jolla, California, USA. [7]Howard Hughes Medical Institute, Salk Institute for Biological Studies, La Jolla, California, USA. Correspondence should be addressed to D.Y.O. (dayoungoh@ucsd.edu) or J.M.O. (jolefsky@ucsd.edu).

Received 10 February; accepted 29 May; published online 6 July 2014; doi:10.1038/nm.3614

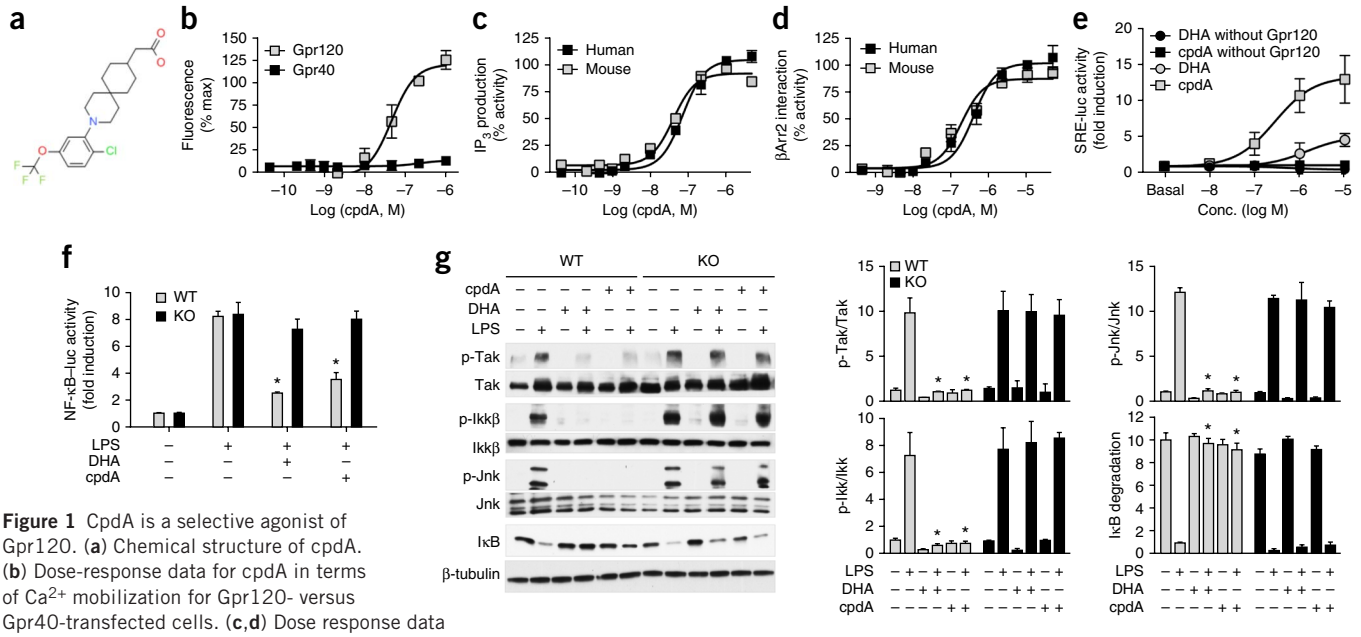

Figure 1 CpdA is a selective agonist of Gpr120. (**a**) Chemical structure of cpdA. (**b**) Dose-response data for cpdA in terms of Ca^{2+} mobilization for Gpr120- versus Gpr40-transfected cells. (**c**,**d**) Dose response data for cpdA in terms of IP_3 production (**c**) and β-arrestin-2 (βArr2) interaction assay (**d**) with human and mouse Gpr120. Results are % activity over basal. (**e**) Gpr120-mediated SRE-luc activity after treatment with either DHA or cpdA for 6 h in HEK 293 cells. For **b**–**e**, data are expressed as mean ± s.e.m. of three independent experiments in triplicate. (**f**) NF-κB–luc activity after pretreatment with DHA and cpdA for 1 h followed by LPS for 6 h in primary macrophages from WT or Gpr120-knockout (KO) mice. Results are fold activities over basal. Each data point represents mean ± s.e.m. of three independent experiments performed in triplicate. $^*P < 0.05$ versus LPS treatment in WT macrophages. $^*P < 0.05$ using two-way analysis of variance (ANOVA) and Bonferroni's *post hoc* test. (**g**) DHA and cpdA inhibits LPS-induced inflammatory signaling in primary macrophages from WT, but not Gpr120-knockout macrophages. The scanned bar graph (right panel) shows fold induction over basal conditions (p-Tak, p-Ikk, and p-Jnk) or LPS treatment (IκB degradation). Data are expressed as the mean ± s.e.m. $^*P < 0.05$ for LPS treatment in WT mice compared to DHA + LPS or cpdA + LPS; two-way ANOVA and Bonferroni's *post hoc* test. $n = 6$ per group. Western blot data are representative of more than five independent experiments.

DHA and cpdA decreased lipopolysaccharide (LPS)-induced NF-κB–reporter gene activity in WT but not Gpr120-knockout primary macrophages (**Fig. 1f**).

To examine Gpr120-mediated anti-inflammatory properties in a more physiologic context, we treated primary macrophages from WT and Gpr120-knockout mice with DHA or cpdA for 1 h, followed by LPS stimulation. DHA and cpdA strongly and comparably inhibited LPS-induced phosphorylation of the inflammatory kinases, Tak1, Ikk-β and Jnk and blocked IκB degradation (**Fig. 1g**). LPS-mediated cytokine secretion and inflammatory gene expression were also inhibited in WT, but not in Gpr120-knockout, primary macrophages (**Supplementary Fig. 1a**,**b**).

Next, we determined whether the synthetic Gpr120 agonist could produce beneficial metabolic effects *in vivo*. We placed WT and Gpr120-knockout mice on a 60% high-fat diet (HFD) for 15 weeks. At this point, we treated separate groups of ten mice each for an additional 5 weeks with 60% HFD alone or HFD containing cpdA at 30 mg per kg^{-1} body weight. The 5-week treatment time point was most effective at improving glucose tolerance and lowering plasma insulin concentration (**Supplementary Fig. 2**). Treatment with the HFD plus cpdA diet led to markedly improved glucose tolerance (**Fig. 2a**) and insulin tolerance (**Fig. 2b**) and decreased insulin secretion compared to HFD alone (**Fig. 2c**) in WT but not Gpr120-knockout mice, with no change in body weight (**Supplementary Fig. 3**). These metabolic effects of cpdA treatment were comparable to dietary ω–3-FA supplementation (**Supplementary Fig. 4**). Notably, during hyperinsulinemic, euglycemic clamp studies, we found that the cpdA-containing HFD caused improved insulin sensitivity with increased glucose infusion rate, enhanced insulin-stimulated glucose disposal rate and a marked increase in the ability of insulin to suppress hepatic glucose production only in WT mice (**Fig. 2d**). This demonstrates the *in vivo* effects of the Gpr120 agonist to produce systemic insulin sensitivity by enhancing muscle and liver insulin action. In addition to improving hepatic insulin sensitivity, cpdA treatment had beneficial effects on hepatic lipid metabolism, causing decreased hepatic steatosis, decreased liver triglyceride levels and diacylglycerols, along with reduced saturated free fatty acid content (**Supplementary Fig. 5**). In contrast, cpdA administration was without effect on hepatic lipid levels in the Gpr120-knockout mice.

Gpr120 can be expressed in enteroendocrine L cells, and earlier studies on Gpr120 have focused on its potential ability to stimulate glucagon-like peptide-1 (Glp-1) secretion[12]. Therefore, we measured total Glp-1 and active Glp-1 levels during oral glucose challenge in HFD-fed mice with or without cpdA treatment (**Supplementary Fig. 6a**). Gpr120 activation did not stimulate Glp-1 secretion at 15 min after oral glucose challenge (**Supplementary Fig. 6a**). Others have also shown a lack of effect of Gpr120 stimulation on Glp-1 secretion[16,17]. We next measured glucose-stimulated insulin secretion (GSIS) in isolated islets from WT and Gpr120-knockout mice (**Supplementary Fig. 6b**) and in a mouse beta cell line, MIN6 (**Supplementary Fig. 6c**). We found that cpdA had a slight, but not statistically significant, effect to increase GSIS in WT islets but was without effect in Gpr120-knockout islets. DHA treatment had a stronger effect to increase GSIS, which was comparable in both WT and Gpr120-knockout islets (**Supplementary Fig. 6b**,**c**), showing that this effect of DHA was independent of Gpr120 but mediated by Gpr40, as previously reported[10,18]. This is also consistent with *in vivo* glucose tolerance test (GTT) results showing slightly higher insulin levels and lower glucose levels in mice given HFD supplemented with ω–3-FA–enriched fish oil compared to cpdA-treated WT mice

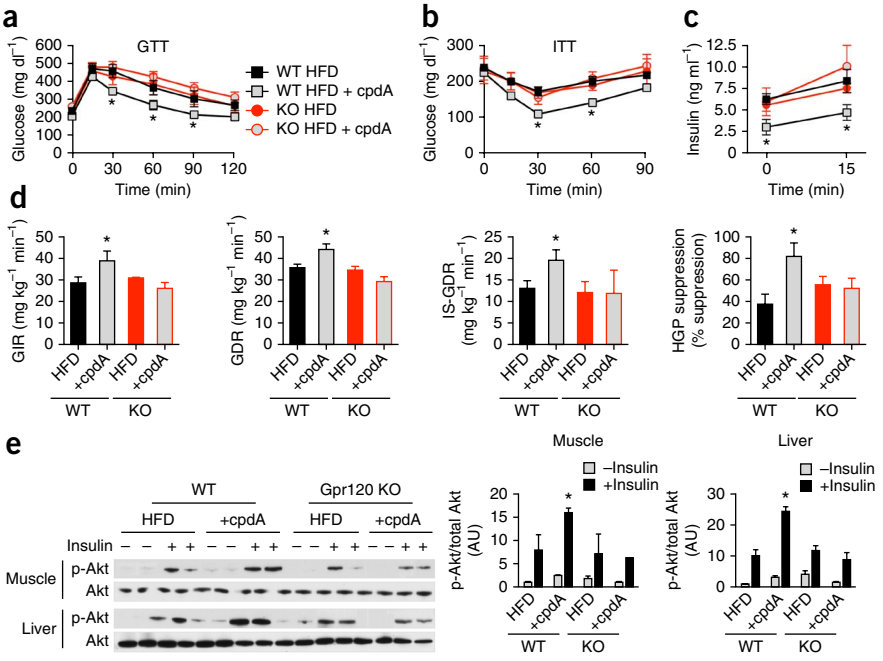

Figure 2 Gpr120 agonist and *in vivo* metabolic studies. (**a**) GTT in WT and Gpr120-knockout mice on HFD or HFD + cpdA. $n = 10$ per group. (**b**) Insulin tolerance test in WT and Gpr120-knockout mice on HFD or HFD + cpdA. $n = 10$ per group. (**c**) Plasma insulin level during GTT at the indicated time points. (**d**) Hyperinsulinemic/euglycemic clamp studies in WT and Gpr120-knockout mice on HFD or HFD + cpdA (+cpdA). Glucose infusion rate (GIR), total glucose disposal rate (GDR), insulin-stimulated glucose disposal rate (IS-GDR) and percentage suppression of hepatic glucose production (HGP) are shown. For **a**–**d**, $^*P < 0.05$ compared to HFD; two-way ANOVA and Bonferroni's *post hoc* test. Data are represented as mean ± s.e.m. mg kg^{-1}, mg per kg body weight. (**e**) Acute insulin response showing phosphorylation of Akt in skeletal muscle and liver from WT and Gpr120-knockout mice on HFD or HFD + cpdA using 0.35 U kg^{-1} insulin injected via inferior vena cava. Left, representative western blot from five independent experiments. Right, fold induction over basal (before insulin injection) conditions. Data are expressed as the mean ± s.e.m. $^*P < 0.05$ versus insulin injection in WT mice on HFD; two-way ANOVA and Bonferroni's *post hoc* test. $n = 6$ per group.

(**Supplementary Fig. 4**). Furthermore, a recent paper by Stone *et al.*[18] showed that Gpr120 is preferentially expressed in mouse islet delta cells and not detected in beta cells and that Gpr120 activation inhibits glucose-induced somatostatin secretion. Therefore, the slight effect of the Gpr120 agonist on GSIS in isolate islets is most likely an indirect effect from inhibition of somatostatin secretion. This interpretation is fully consistent with our results showing that cpdA has no effect on GSIS in MIN6 cells.

We performed acute insulin response studies by measuring Akt phosphorylation in muscle and liver after an injection of insulin into HFD-fed WT or Gpr120-knockout mice. Fully consistent with the *in vivo* glucose clamp studies, this biochemical measure of muscle and hepatic insulin signaling was increased with cpdA treatment in WT but not Gpr120-knockout mice (**Fig. 2e**). Taken together, these results show that the Gpr120 agonist leads to increased systemic insulin sensitivity *in vivo*.

Gpr120 stimulation by ω–3-FAs decreases adipose tissue macrophage (ATM) infiltration and reduces inflammatory gene expression[8]. Consistent with this, we observed that cpdA treatment blocked chemotaxis of WT mouse macrophages induced by adipocyte-derived conditioned medium as effectively as DHA treatment, but both cpdA and DHA were without effect in Gpr120-knockout macrophages (**Fig. 3a**).

To determine whether these *in vitro* chemotaxis results translated to the *in vivo* situation, we directly measured macrophage migration into adipose tissue using an *in vivo* macrophage tracking technique. With this approach, we obtained circulating monocytes from WT donor mice and labeled them with fluorescent PKH26 dye *ex vivo*. We then injected the labeled monocytes into recipient HFD-fed WT and Gpr120-knockout mice with or without dietary ω–3-FA supplementation or cpdA treatment. There was a substantial decrease in labeled ATM appearance in both ω–3-FA–treated and cpdA–treated WT mice, but there was no effect in Gpr120-knockout mice (**Fig. 3b**). These data were even more revealing when we examined the subpopulations of labeled macrophages between the groups. ATMs expressing Cd11c are M1-like and proinflammatory (ATM1) compared to M2-like Cd11c-negative ATMs (ATM2), which are noninflammatory. With this analysis, there was an even greater decrease in the number of recruited Cd11c-positive ATMs in both ω–3-FA–treated and cpdA–treated WT mice. At the same time, there was an increase in the Cd11c-negative ATM population in the cpdA-treated and ω–3-FA–treated WT mice, with no effect in Gpr120-knockout mice (**Fig. 3b**). This shows that cpdA led to reduced monocyte migration with less M1-like Cd11c-positive ATMs and that the labeled monocytes that do become ATMs favor the M2-like Cd11- negative state. Along with *in vivo* migration results, we also found reduced ATM content by immunohistochemistry (F4/80 staining) in adipose tissue sections from cpdA-treated compared to HFD-fed WT mice (**Fig. 3c**). This was accompanied by decreased numbers of Cd11c-positive ATMs and increased numbers of Cd11c-negative ATMs (**Fig. 3d** and **Supplementary Fig. 7a**) by FACS analysis. As before, all of these effects were observed in WT but not Gpr120-knockout mice.

Although macrophages are one of the crucial immune cells mediating HFD-induced inflammation, recent studies have shown that other immune cell types, such as T cells and B cells, can contribute to adipose tissue inflammation[19,20]. In particular, Foxp3$^+$ regulatory T (T_{reg}) cells[19] and regulatory B (B_{reg}) cells[20] suppress inflammation in adipose tissue and can secrete interleukin-10 (**Fig. 3e**). Therefore, we measured T_{reg} and B_{reg} cell abundance in HFD-fed WT and Gpr120-knockout mice with or without cpdA treatment and found increased abundance of T_{reg} and B_{reg} cells in adipose tissue from cpdA-treated WT mice but not Gpr120-knockout mice (**Supplementary Fig. 7b**,**c**). Taken together, our results suggest the ratio of proinflammatory M1-like ATMs to anti-inflammatory M2-like ATMs and T_{reg} and B_{reg} cells are markedly decreased with cpdA treatment, and this ability of Gpr120 agonism to boost adipose tissue T_{reg} cell and B_{reg} cell levels may represent an additional therapeutic effect.

We also found decreased expression of a number of proinflammatory genes in mouse epididymal adipose tissue, such as *Tnf*, *Il6*, *Ccl2* (also known as *Mcp1*) and *Il1b* (**Fig. 3e**). At the same time, we

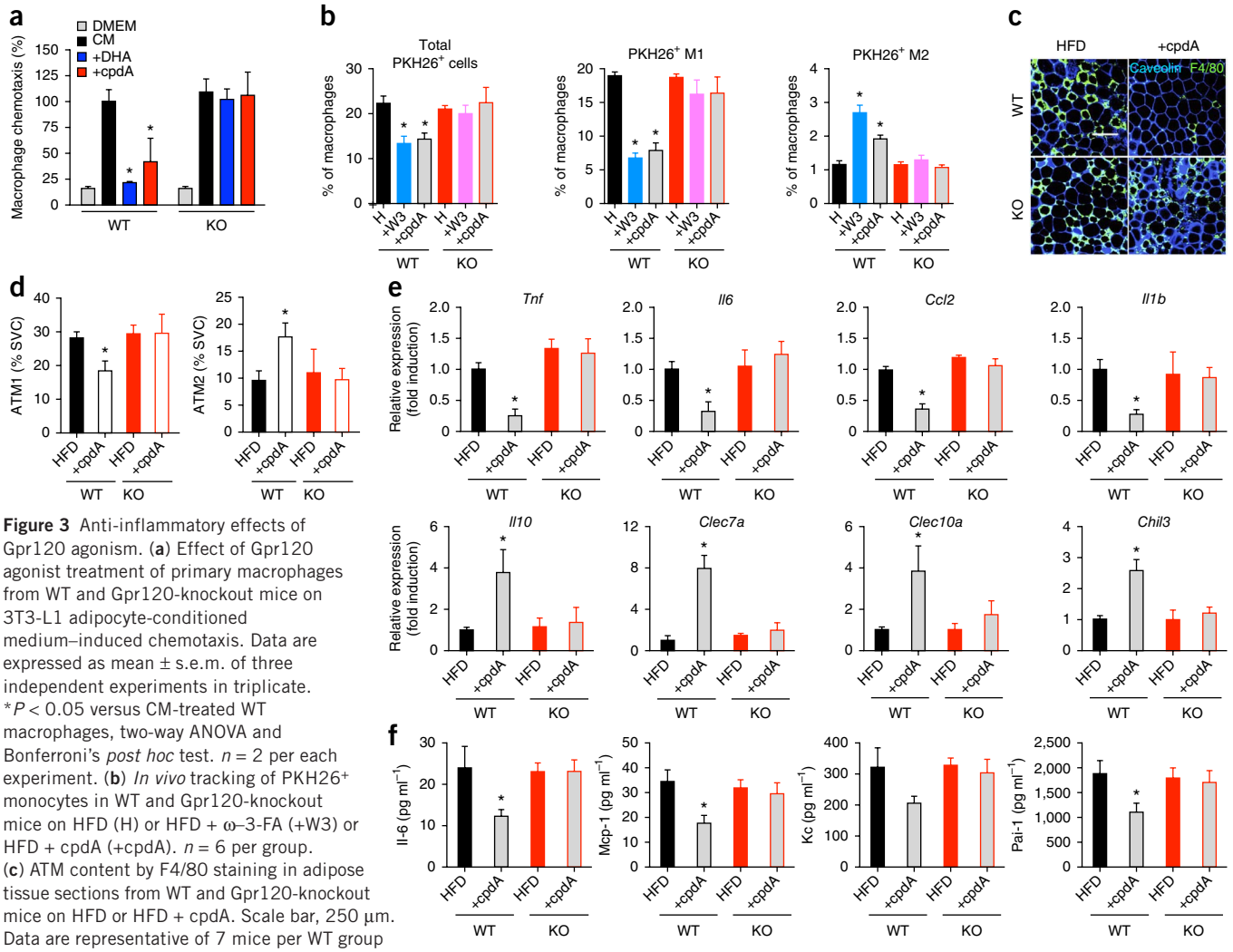

Figure 3 Anti-inflammatory effects of Gpr120 agonism. (**a**) Effect of Gpr120 agonist treatment of primary macrophages from WT and Gpr120-knockout mice on 3T3-L1 adipocyte-conditioned medium–induced chemotaxis. Data are expressed as mean ± s.e.m. of three independent experiments in triplicate. $^*P < 0.05$ versus CM-treated WT macrophages, two-way ANOVA and Bonferroni's *post hoc* test. $n = 2$ per each experiment. (**b**) *In vivo* tracking of PKH26$^+$ monocytes in WT and Gpr120-knockout mice on HFD (H) or HFD + ω–3-FA (+W3) or HFD + cpdA (+cpdA). $n = 6$ per group. (**c**) ATM content by F4/80 staining in adipose tissue sections from WT and Gpr120-knockout mice on HFD or HFD + cpdA. Scale bar, 250 µm. Data are representative of 7 mice per WT group and 8 mice per Gpr120-knockout group. (**d**) FACS analysis of ATMs from WT and Gpr120-knockout mice on HFD or HFD + cpdA. $n = 6$ per group. (**e**) Relative mRNA level of inflammatory cytokines (top) and anti-inflammatory cytokines (bottom) in adipose tissue from WT and Gpr120-knockout mice on HFD or HFD + cpdA. $n = 10$ per group. (**f**) Serum interleukin-6 (Il-6), monocyte chemoattractant protein-1 (Mcp-1), Kc, and plasminogen activator inhibitor-1 (Pai-1) levels from WT and Gpr120-knockout mice on HFD or HFD + cpdA. $n = 10$ per group. For **b**,**d**–**f**, data are expressed as the mean ± s.e.m. $^*P < 0.05$ versus WT mice on HFD; two-way ANOVA and Bonferroni's *post hoc* test.

observed an increase in expression of anti-inflammatory genes, such as *Il10*, *Clec7a*, *Clec10a* (also known as *Mgl1*) and *Chil3* (also known as *Ym1*) (**Fig. 3e**). Notably, adipose tissue levels of the proinflammatory arachidonic acid metabolites leukotriene B4 (LTB4), prostaglandin E_2 (PGE_2), 5- hydroxyeicosatetraenoic acid (5-HETE) and leukotriene A4 (LTA4) were also inhibited by both ω–3-FA and cpdA treatment (**Supplementary Fig. 8**). Indicative of systemic inflammation, circulating cytokine levels are elevated in obesity, and inflammatory cytokine levels were markedly reduced in HFD-fed, cpdA-treated WT mice but not in HFD-fed Gpr120-knockout mice (**Fig. 3f**).

To directly link these observations to inflammatory transcriptional output, we performed RNA sequencing (RNA-seq) analyses in primary macrophages from WT and Gpr120-knockout mice. Pretreatment of WT macrophages with DHA or cpdA inhibited LPS-stimulated inflammatory gene expression, but this was not the case in Gpr120-knockout macrophages (**Supplementary Fig. 9a**). Information clustering results revealed that highly significantly down-regulated biological processes (Bonferroni's P value < 0.01) in LPS-stimulated macrophages pretreated with DHA (**Supplementary Fig. 9b**) or cpdA (**Supplementary Fig. 9c**) included several inflammation-related pathways.

It is known that nitric oxide (NO) can attenuate insulin signaling through nitrosylation of insulin signaling molecules, including Akt[21]. Tissue NO levels represent the balance between inducible nitric oxide synthase (iNOS) and arginase activity. *Nos2* (encoding iNOS) mRNA expression was induced in adipose tissue from both WT and Gpr120-knockout mice by HFD, and this effect was reduced by cpdA treatment in WT but not Gpr120-knockout mice (**Fig. 4a**). HFD also led to increased *Arg1* (encoding arginase) expression, and this increase was enhanced in WT mice, but not Gpr120-knockout mice, with cpdA treatment (**Fig. 4a**). Thus, the iNOS/arginase ratio was markedly reduced in WT adipose tissue by HFD plus cpdA compared to HFD alone (**Fig. 4a**). As would be predicted from these gene expression changes, levels of adipose tissue NO_2, a stable breakdown product of NO, were reduced by ~60% in HFD-fed WT mice treated with cpdA (**Fig. 4b**). This decrease was almost completely abrogated in Gpr120-knockout mice. Consistent with these changes in NO levels, nitrosylation of Akt was increased in both adipose tissue from WT

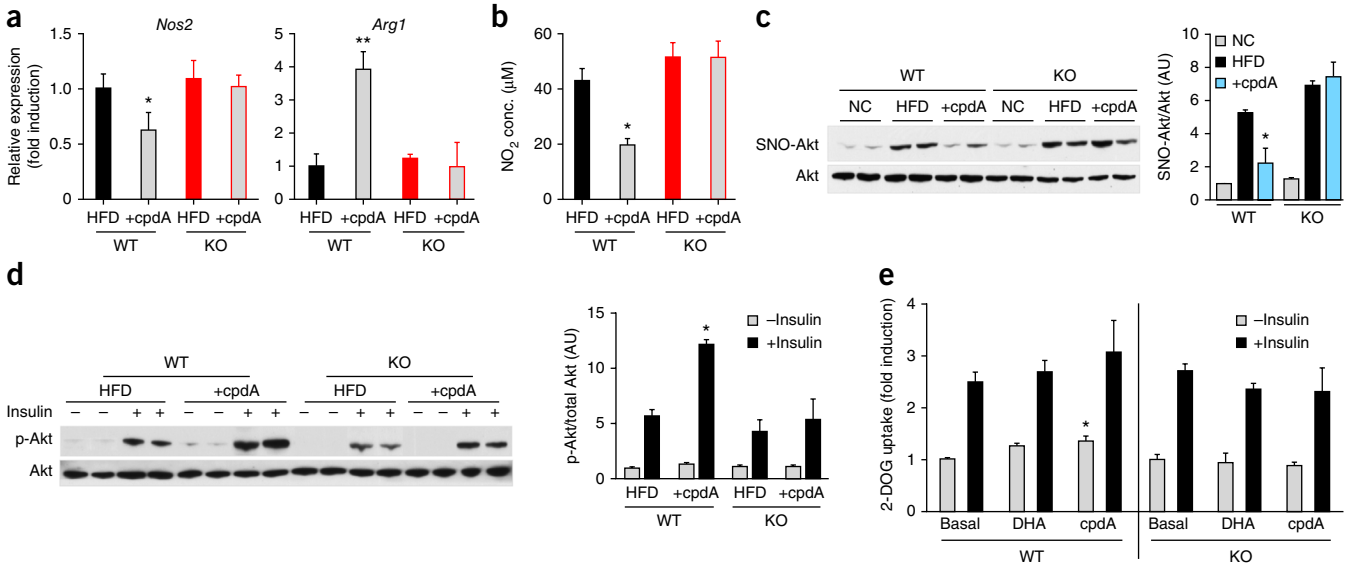

Figure 4 Production of NO and glucose uptake in adipocytes. (**a**) mRNA levels of *Nos2* and *Arg1* in adipose tissue from WT and Gpr120-knockout mice on HFD or HFD + cpdA. $n = 10$ per group. (**b**) Nitric oxide level in adipose tissue of WT and Gpr120-knockout mice on HFD or HFD + cpdA. $n = 8$ per group. (**c**) Left, western blot showing HFD-induced nitrosylation of Akt in adipose tissue; representative of five independent experiments. Right, fold induction over normal chow (NC) condition. For **a**–**c**, $^*P < 0.05$ versus WT mice on HFD; two-way ANOVA and Bonferroni's *post hoc* test. (**d**) Akt phosphorylation in adipose tissue from WT or Gpr120-knockout mice on HFD or HFD + cpdA before and after insulin injection. Left, representative western blot from three independent experiments. Right, fold induction over basal (before insulin injection). $n = 6$ per group. $^*P < 0.05$ versus insulin injection in WT mice on HFD; two-way ANOVA and Bonferroni's *post hoc* test. (**e**) Glucose uptake in primary adipocytes from WT and Gpr120-knockout mice pretreated with DHA or cpdA for 30 min and subsequently incubated in the absence and presence of insulin, followed by measurement of 2-deoxyglucose (2-DOG) uptake. Data are expressed as the mean ± s.e.m. from three independent experiments. $^*P < 0.05$ over basal; two-way ANOVA and Bonferroni's *post hoc* test.

and Gpr120-knockout mice on HFD, and this was reduced by cpdA treatment only in WT adipose tissue (**Fig. 4c**). Concomitant with this, insulin-stimulated Akt phosphorylation was greater in adipose tissue from cpdA-treated WT mice on HFD compared to that from WT mice on HFD alone (**Fig. 4d**).

To further examine the effect of cpdA on insulin signaling, we isolated primary adipocytes from WT and Gpr120-knockout mice for glucose uptake analyses. Ligand stimulation of Gpr120 led to a modest increase in glucose uptake in primary WT adipocytes but did not have any effect in Gpr120-knockout adipocytes (**Fig. 4e**). As previously described for ω–3-FAs, Gpr120 agonist–mediated glucose uptake was dependent on Gαq/11 signaling and independent of the β-arrestin-2 pathway (**Supplementary Fig. 10** and ref. 8).

Recently, the ω–3-FA–sensing GPCR, Gpr120, has received increasing interest as a therapeutic target for the treatment of both metabolic and inflammatory diseases. Knockout experiments in cells and mice, as well as human genetic studies, are consistent with the view that Gpr120 plays an important role in anti-inflammation and insulin sensitization[8,9,12]. Despite this interest, further validation of Gpr120 as a therapeutic target has been hindered by the lack of available small-molecule agonists. In our current work, we have used a new orally available small-molecule agonist for Gpr120, cpdA, to explore the pharmacology and function of Gpr120 *in vitro* and *in vivo*. Comparison of cpdA with ω–3-FAs clearly demonstrated that this Gpr120 agonist is a selective and potent activator of both human and mouse Gpr120. Most importantly, treatment with this compound *in vitro* and *in vivo* caused anti-inflammatory insulin-sensitizing effects, comparable to ω–3-FA administration. Taken together, Gpr120 agonists could become future insulin-sensitizing agents for the treatment of type 2 diabetes and other human insulin-resistant states.

METHODS

Methods and any associated references are available in the online version of the paper.

Accession codes. Sequencing data have been deposited in NCBI high-throughput sequence database with accession code GSE58282.

Note: Any Supplementary Information and Source Data files are available in the online version of the paper.

ACKNOWLEDGMENTS

This study was funded in part by grants to J.M.O. (DK033651, DK074868, DK063491 and DK09062) and D.Y.O. (P30 DK063491), a grant from Merck, Inc. to J.M.O. and D.Y.O., Austrian science fund (FWF Doktoratskolleg DK-MCD W1226 and the FWF project P24143) to J.G.B.-S., and a Marshall Plan Scholarship to A.R.P. We thank A. Tyler for editorial assistance and N. Sekiya for assistance with FACS analysis at the Veterans Affairs San Diego hospital, the University of California, San Diego (UCSD) Histology Core lab for technical help with processing liver specimens, and the UCSD Microscope Resource for microscopy analysis, which is funded by UCSD Neuroscience Microscopy Shared Facility Grant P30 NS047101.

AUTHOR CONTRIBUTIONS

D.Y.O. designed the studies and performed most of the experiments; E.W. assisted with all animal experiments, FACS analysis and gene expression measurements; W.S.L. and D.L. conducted hyperinsulinemic-euglycemic clamps; T.E.A., J.M.C., M.A.P., J.D.S. and C.S. developed cpdA and provided initial screening data; A.R.P., H.C. and T.J.C. assisted with animal experiments and gene expression measurements; R.S. and N.H. carried out RNA-seq data analysis; S.M.W. performed lipomics analysis; A.M.A. and O.Q. performed eicosanoids measurements; J.M. conducted GSIS experiments; R.M.E. and J.G.B.-S. contributed to discussion; D.Y.O. and J.M.O. analyzed, interpreted data, supervised the project and co-wrote the manuscript.

COMPETING FINANCIAL INTERESTS

The authors declare no competing financial interests.

1. Sijben, J.W. & Calder, P.C. Differential immunomodulation with long-chain *n*-3 PUFA in health and chronic disease. *Proc. Nutr. Soc.* **66**, 237–259 (2007).
2. Lee, J.Y. *et al.* Differential modulation of Toll-like receptors by fatty acids: preferential inhibition by *n*-3 polyunsaturated fatty acids. *J. Lipid Res.* **44**, 479–486 (2003).
3. Proudman, S.M., Cleland, L.G. & James, M.J. Dietary omega-3 fats for treatment of inflammatory joint disease: efficacy and utility. *Rheum. Dis. Clin. North Am.* **34**, 469–479 (2008).
4. Calder, P.C. Polyunsaturated fatty acids and inflammation. *Biochem. Soc. Trans.* **33**, 423–427 (2005).
5. Polozova, A. & Salem, N. Jr. Role of liver and plasma lipoproteins in selective transport of *n*-3 fatty acids to tissues: a comparative study of ^{14}C-DHA and ^{3}H-oleic acid tracers. *J. Mol. Neurosci.* **33**, 56–66 (2007).
6. Neschen, S. *et al. n*-3 Fatty acids preserve insulin sensitivity *in vivo* in a peroxisome proliferator–activated receptor-α–dependent manner. *Diabetes* **56**, 1034–1041 (2007).
7. Geleijnse, J.M., Giltay, E.J., Grobbee, D.E., Donders, A.R. & Kok, F.J. Blood pressure response to fish oil supplementation: metaregression analysis of randomized trials. *J. Hypertens.* **20**, 1493–1499 (2002).
8. Oh, D.Y. *et al.* GPR120 is an omega-3 fatty acid receptor mediating potent anti-inflammatory and insulin-sensitizing effects. *Cell* **142**, 687–698 (2010).
9. Ichimura, A. *et al.* Dysfunction of lipid sensor GPR120 leads to obesity in both mouse and human. *Nature* **483**, 350–354 (2012).
10. Itoh, Y. *et al.* Free fatty acids regulate insulin secretion from pancreatic beta cells through GPR40. *Nature* **422**, 173–176 (2003).
11. Hudson, B.D. *et al.* The pharmacology of TUG-891, a potent and selective agonist of the free fatty acid receptor 4 (FFA4/GPR120), demonstrates both potential opportunity and possible challenges to therapeutic agonism. *Mol. Pharmacol.* **84**, 710–725 (2013).
12. Hirasawa, A. *et al.* Free fatty acids regulate gut incretin glucagon-like peptide-1 secretion through GPR120. *Nat. Med.* **11**, 90–94 (2005).
13. Hara, T. *et al.* Novel selective ligands for free fatty acid receptors GPR120 and GPR40. *Naunyn Schmiedebergs Arch. Pharmacol.* **380**, 247–255 (2009).
14. Shimpukade, B., Hudson, B.D., Hovgaard, C.K., Milligan, G. & Ulven, T. Discovery of a potent and selective GPR120 agonist. *J. Med. Chem.* **55**, 4511–4515 (2012).
15. Sun, Q. *et al.* Structure-activity relationships of GPR120 agonists based on a docking simulation. *Mol. Pharmacol.* **78**, 804–810 (2010).
16. Paulsen, S.J. *et al.* Expression of the fatty acid receptor GPR120 in the gut of diet-induced-obese rats and its role in GLP-1 secretion. *PLoS ONE* **9**, e88227 (2014).
17. Xiong, Y. *et al.* Activation of FFA1 mediates GLP-1 secretion in mice. Evidence for allosterism at FFA1. *Mol. Cell. Endocrinol.* **369**, 119–129 (2013).
18. Stone, V.M. *et al.* GPR120 (FFAR4) is preferentially expressed in pancreatic delta cells and regulates somatostatin secretion from murine islets of Langerhans. *Diabetologia* **57**, 1182–1191 (2014).
19. Feuerer, M. *et al.* Lean, but not obese, fat is enriched for a unique population of regulatory T cells that affect metabolic parameters. *Nat. Med.* **15**, 930–939 (2009).
20. Nishimura, S. *et al.* Adipose natural regulatory B cells negatively control adipose tissue inflammation. *Cell Metab.* **18**, 759–766 (2013).
21. Yasukawa, T. *et al.* S-nitrosylation–dependent inactivation of Akt/protein kinase B in insulin resistance. *J. Biol. Chem.* **280**, 7511–7518 (2005).

ONLINE METHODS

Chemicals and reagents. CpdA was provided by Merck & Co., Inc. (Whitehouse Station, NJ), and DHA was from Cayman Chemical (Ann Arbor, MI). All other chemicals were purchased from Sigma unless mentioned otherwise.

Animal care and use. Male C57BL/6 WT or Gpr120-knockout littermates were fed a normal chow (13.5% fat; LabDiet) or high-fat diet (60% fat; Research Diet) *ad libitum* for 15–20 weeks from 8 weeks of age. Gpr120-knockout mice and WT littermates were initially provided by Taconic, Inc. (Hudson, NY) and bred further in house, backcrossing with C57BlL6J mice for >10 generations. After 15 weeks on HFD, WT and Gpr120-knockout male mice were switched to an isocaloric HFD supplemented with ω–3-FA concentrate[8] or 30 mg kg^{-1} cpdA and fed for 5 weeks. Mice received a fresh diet every third day, and food consumption and body weight were monitored. Animals were housed in a specific pathogen–free facility and given free access to food and water. All procedures were approved by the University of California, San Diego Animal Care and Use Committee. *In vivo* metabolic studies were performed as described previously[8].

Metabolic studies. We performed GTT, ITT and hyperinsulinemic euglycemic clamp studies as described[8,22].

Acute insulin response. WT and Gpr120-knockout mice on HFD or HFD + cpdA were injected with insulin (0.35 U kg^{-1}) after a 6-h fast into the inferior vena cava. Tissue species were harvested as described[23], at the indicated time points, and flash frozen in liquid N_2. We prepared lysates and ran western blots according to standard protocols.

Western blotting and gene expression analyses. Western blotting and quantitative PCR (qPCR) were performed as previously described[8,22]. The antibodies used were to phospho-Tak1 (90C7, 1:1,000), Tak1 (D94D7, 1:1,000), phospho-Ikkα/β (16A6, 1:500), Ikkβ (D30C6, 1:1,000), phospho-Jnk (81E11, 1:1,000), Jnk (56G8, 1:1,000), IkB (44D4, 1:1,000), phospho-Akt (587F11, 1:1,000), Akt (11E7, 1:1,000) and β-tubulin (#2146, 1:2,000); all were from Cell Signaling Technology.

SVCs isolation and FACS analysis. SVC isolation and FACS analyses were performed as previously described[24]. SVCs were incubated with Fc Block (BD Biosciences) for 20 min at 4 °C before staining with fluorescently labeled primary antibodies or control IgGs for 30 min at 4 °C. We used Aqua L-D (Invitrogen) to exclude dead cells. The antibodies used were to F4/80-APC (BM8, AbD Serotec, 1:100), Cd11b-FITC (M1/70, BD Biosciences. 1:100), Cd11c-PE (HL-3, BD Biosciences, 1:50), Cd4 (RM4-5, BD Biosciences, 1:50), Cd19 (MB19-1, eBioscience, 1:50), Cd22.2 (CY34.1, BD Biosciences, 1:25), Cd25 (PC61, eBioscience, 1:50), Cd45R-APC-Cy7 (BD Biosciences, 1:50) and Foxp3 (FJK-16s, eBioscience, 1:50). Unstained, single-stained and fluorescence-minus-one controls were used for setting compensation and gates.

Immunohistochemistry. Liver was fixed and embedded in paraffin and sectioned for H&E staining.

***In vitro* chemotaxis assay.** *In vitro* chemotaxis assay was performed as previously described[8].

***In vivo* macrophage tracking.** *In vivo* macrophage tracking was performed as previously described[25]. Briefly, blood leukocytes from C57BL/6 WT mice were subjected to red blood cell lysis, and monocyte subsets were enriched with EasySep mouse monocyte enrichment kit (STEMCELL Tech, Vancouver, BC) following the manufacturer's instructions. Isolated monocytes (2×10^6 to 5×10^6) were washed once in serum-free medium (RPMI-1640) and suspended in 2 ml of Diluent solution C (included in the PKH26 labeling kit). Two ml of PKH26 (Sigma Chemical Co., St. Louis, MO) at 2×10^{-3} M in Diluent C were added and mixed, and the cells were incubated for 10 min at room temperature in the dark. The staining reaction was stopped by addition of an equal volume (2 ml) of medium supplemented with 10% FBS. The mixture was centrifuged and the cells were washed once and resuspended in serum-containing medium. Subsequent to labeling with PKH26, the monocytes were counted, and ~0.2×10^6 viable cells were suspended in 0.2 ml PBS and injected retro-orbitally in each group of mice. Five days after injection, the ATMs were isolated from visceral fat tissue and analyzed by FACS[25].

Glucose uptake in primary adipocyte and 3T3-L1 adipocytes. Glucose uptake in primary adipocytes and 3T3-L1 adipocytes were measured as previously described[8,23].

Intraperitoneal primary macrophage isolation and culture. We harvested primary macrophages from WT and Gpr120-knockout mice as described[8]. Three days after harvest and plating, we pretreated cells with 100 μM DHA or 10 μM cpdA for 1 h, followed by LPS (100 ng ml^{-1}) for 15 min before protein isolation, LPS for 6 h to collect condition medium and RNA isolation for qPCR analyses. The NF-κB–luc reporter assay was conducted as described[26] with primary macrophages from WT and Gpr120-knockout mice.

Nitrate measurement. Nitrate content in adipose tissue lysate was measured using the Griess Reagent System (Promega) in accordance with the manufacturer's protocol.

Measurement of protein nitrosylation. S-nitrosylation of Akt was detected using the biotin-switch method (Cayman) according to the manufacturer's protocol.

Lipid measurement. Lipid measurements in mouse liver were performed by Lipomics as described previously[8].

LTB4 measurement. LTB4 measurement in mouse adipose tissue was performed as previously described[27].

Measurement of insulin secretory response from isolated islets. Glucose-stimulated insulin secretion from mouse islets was assessed as previously described[28]. For static GSIS assays, ~20 mouse islets were incubated for 2 h in low-glucose medium at 37 °C, 5% CO_2, and then incubated for 60 min or 75 min with 2.8 mM or 16.7 mM glucose in the same conditions.

RNA library construction and high-throughput sequencing. RNA library construction and Illumina high-throughput sequencing were performed as described previously[29].

Processing RNA-seq data for information clustering and heatmap. RNA sequences from Illumina HiSeq were aligned to the mouse transcriptome using the Bowtie2 aligner[30]. Gene-level count summaries were analyzed for statistically significant changes using DESeq[31]. Individual *P* values were adjusted for multiple testing by calculating the *q* values. For each gene, the *q* value is the smallest false discovery rate at which the gene is found significant. For information clustering and heatmap generation, we analyzed biological processes as defined by the Gene Ontology Consortium[32]. A typical list of significant biological processes usually contains several redundant, closely related gene sets with great overlap of member genes. In order to reduce redundancy of reporting, we cluster the significant terms using a true distance metric called variation of information[33]. Qualitatively speaking, variation of information between two sets of genes is smaller (i.e., gene sets are closer) when the gene sets share a large fraction of member genes and is larger (gene sets are farther apart) when the gene memberships have less overlap. A distance matrix thus obtained defines a graph in higher-dimensional Euclidean space in which each node is a gene set and the length of every edge is the distance (variation of information) between the connected nodes. This graph is then optimally visualized in two dimensions using a Principal Coordinates Analysis (multi-scaling) function cmdscale of the R language. For presentation purposes, we choose to represent each node (gene set) not just by a point but by a circle whose diameter is proportional to the –log of the Bonferroni-adjusted *P* value. This way, more significant nodes appear as larger circles to draw attention.

Any two circles may appear to overlap, but this should not be interpreted in the usual Venn diagram sense. When circles overlap, it is because the gene sets they represent were close enough in the information sense (had overlapping gene membership) and were significant enough to produce large circles. We use this visualization to report the relevant nonredundant biological processes.

Data analyses. Densitometric quantification and normalization were performed using the ImageJ 1.42q software. The values presented are expressed as the means ± s.e.m. The statistical significance of the differences between various treatments was determined by one-way analysis of variance with the Bonferroni correction using GraphPad Prism 6.0 (San Diego, CA). $P < 0.05$ was considered significant. No statistical method was used to predetermine sample size. The experiments were not randomized. The investigators were not blinded to allocation during experiments and outcome assessment.

22. Li, P. *et al.* Adipocyte NCoR knockout decreases PPARγ phosphorylation and enhances PPARγ activity and insulin sensitivity. *Cell* **147**, 815–826 (2011).
23. Talukdar, S. *et al.* Neutrophils mediate insulin resistance in mice fed a high-fat diet through secreted elastase. *Nat. Med.* **18**, 1407–1412 (2012).
24. Li, P. *et al.* Functional heterogeneity of CD11c-positive adipose tissue macrophages in diet-induced obese mice. *J. Biol. Chem.* **285**, 15333–15345 (2010).
25. Oh, D.Y., Morinaga, H., Talukdar, S., Bae, E.J. & Olefsky, J.M. Increased macrophage migration into adipose tissue in obese mice. *Diabetes* **61**, 346–354 (2012).
26. Li, P. *et al.* NCoR repression of LXRs restricts macrophage biosynthesis of insulin-sensitizing omega 3 fatty acids. *Cell* **155**, 200–214 (2013).
27. Quehenberger, O. *et al.* Lipidomics reveals a remarkable diversity of lipids in human plasma. *J. Lipid Res.* **51**, 3299–3305 (2010).
28. Lee, Y.S. *et al.* The fractalkine/CX3CR1 system regulates beta cell function and insulin secretion. *Cell* **153**, 413–425 (2013).
29. Lister, R. *et al.* Hotspots of aberrant epigenomic reprogramming in human induced pluripotent stem cells. *Nature* **471**, 68–73 (2011).
30. Langmead, B. & Salzberg, S.L. Fast gapped-read alignment with Bowtie 2. *Nat. Methods* **9**, 357–359 (2012).
31. Anders, S. & Huber, W. Differential expression analysis for sequence count data. *Genome Biol.* **11**, R106 (2010).
32. Reference Genome Group of the Gene Ontology Consortium. The Gene Ontology's Reference Genome Project: a unified framework for functional annotation across species. *PLoS Comput. Biol.* **5**, e1000431 (2009).
33. Nugent, R. & Meila, M. An overview of clustering applied to molecular biology. *Methods Mol. Biol.* **620**, 369–404 (2010).

doi:10.1038/nm.3614